Bull. Mater. Sci. (2021) 44:280
https://doi.org/10.1007/s12034-021-02590-4

Anomalous electrical transport in orientationally controlled trinary hybrids of graphene and twisted bilayer molybdenum disulphide

SHAILI SETT[1,*], SUDIPTA KUNDU[1], SALONI KAKKAR[1], NAVKIRANJOT KAUR GILL[1], MANISH JAIN[1] and ARINDAM GHOSH[1,2]

[1]Department of Physics, Indian Institute of Science, Bangalore 560012, India
[2]Centre for Nano Science and Engineering, Indian Institute of Science, Bangalore 560012, India
*Author for correspondence (shailisett@iisc.ac.in)

MS received 14 July 2021; accepted 14 September 2021

Abstract. Moiré superlattices of two-dimensional (2D) materials oriented at low twist angles generate a large-scale interference pattern leading to strong interlayer coupling, which influences the band structure and introduces flatbands. Conventional electronic transport measurements have shown the effects of flatband physics, manifesting as correlated insulating states and emergent superconductivity. In this study, we probe the electronic states in a trinary hybrid of graphene and twisted bilayer (tbl) MoS_2. Graphene acts as a sensing layer, which captures the electronic effects of the underlying substrate, and we observe certain anomalies in the electronic characteristics of graphene only in the presence of an underlying 58.5° tbl MoS_2, at low temperatures. Interestingly, graphene on tbl MoS_2, with twist angle near 0° or on natural bilayer MoS_2, does not show any anomalies. Density functional theory calculations show several distinguishable peaks in the density of states at the conduction band edge of twisted MoS_2 near 60°. We speculate that the anomaly appears due to fermi level pinning of graphene owing to a large density of states in the flatbands of twisted bilayer MoS_2. An analysis of the energetics in the graphene-MoS_2 hybrid quantitatively agree with theoretical predictions.

Keywords. Graphene; transition metal dichalcogenide; heterostructure; flatbands; moiré superlattice.

1. Introduction

Emergent phenomena enabled by moiré patterns in an artificial lattice are currently of great interest, both theoretically [1–4] and experimentally [5–9]. Moiré superlattices (MSL) comprise of an orientationally controlled heterostructure of two-dimensional (2D) materials, formed by the angular mismatch between two similar lattices or by two dissimilar lattices with nearly equal lattice constants. The relative rotation in between the adjacent layers, or the twist angle (θ) between them plays a crucial role in changing the electronic band structure of the superlattice. In case of graphene (Gr), it opens up a single particle gap at the gamma point of the Moiré Brillion Zone and introduces flatbands; bands which have a reduced bandwidth (W) of $\leq$ 10 meV [8,9]. This leads to a large ratio U/W, where U is the on-site Coulomb repulsion energy suggesting the possibility of correlated states and other emergent phenomena. Such flatbands have been well explored in twisted graphene-based systems and show correlated insulating states, superconducting states and topological states. Superconductivity appears in magic-angle twisted bilayer (tbl) graphene within a very narrow twist angle $\sim$1.1° [9]. In MSL of transition metal dichalcogenides (TMDCs), the twist angle range is more relaxed which provides practical advantages in fabrication [3]. Flattening of the bandwidth upto 1 meV occurs for twist angles $>$ 56.5° for tbl MoS_2, which has been predicted theoretically [3]. In tbl WSe_2, it has been recently predicted that flatbands (at low twist angles near 0°) near the valence band maxima show non-trivial Chern number [4,10]. Experiments investigating novel strongly correlated physics of electrons in artificially created twisted TMDCs are limited. Existence of flatbands in the electronic structure of a 57.5° twisted WSe_2 was shown using scanning tunnelling spectroscopy [11]. Recently, correlated insulating state (at half filling), metallic behaviour (far from half filling) as well as superconductivity (at about half filling) were claimed in low-angle twisted WSe_2 [12]. Correlated insulating states have also been observed at fractional fillings of heterobilayers of WSe_2/WS_2 MSL [13].

First-principles density functional theory calculations on tbl MoS_2 show large structural reconstructions, leading to

This article is part of the special issue on 'Quantum materials and devices'.

Supplementary Information: The online version contains supplementary material at https://doi.org/10.1007/s12034-021-02590-4.

Published online: 16 November 2021

the formation of shear soliton and ultra-flatbands at the band edge [3,14]. The MSL of TMDCs consists of different atomic stackings, which have different energies and interlayer separations. The difference in the energy of these stackings drives the relaxation and the relaxed pattern is determined by the stacking energy gain and strain energy cost. The interlayer separation has a variation of 0.5 Å in the MSL and the local interlayer separation influences the hybridization of the gamma point states. The local hybridization along with the effective moiré potential (includes both interlayer potential and intralayer potential) determines the localization of flatbands. Twisted bilayer MoS_2 (or any other tbl TMDC) forms two distinguishable MSLs for twist angles near 0° and near 60°. This is because the Mo and S atoms belong to two different sublattices, leading to sublattice symmetry breaking. In these artificial structures, several ultra-flatbands form at the valence and conduction band edges, which are well separated in energy. Till date, there has been no experimental confirmation of flatbands in tbl MoS_2 or any emergent phenomena that arise due to hybridization of the band structure.

van der Waals coupling of graphene to tbl TMDCs provides a new transport-based route to explore the electronic states in the tbls. Earlier, graphene/TMDC heterostructures have been widely used in optoelectronic devices, where photogating effect due to charge capture at the TMDC/dielectric interface and charge transfer to graphene leads to ultra-high photoresponse [15,16]. Due to suitable band alignment of graphene with the TMDC, inter-layer charge transfer is possible, occurring with picosecond timescales. Sandwiching a hexagonal boron nitride (hBN) layer, in between the Gr/MoS_2 photodetector, shows an increase in the charge decay time, which can be controlled by the hBN thickness [17]. Recently, a resonant inter-layer electron transfer has been observed in these heterostructures, by externally tuning the fermi level (E_F) of graphene to match the excitonic state of the TMDC [18]. It provides an insight into the exciton dissociation process and outlines a new way to determine the exciton binding energy in TMDCs that can be obtained by tuning E_F of graphene. Another interesting observation in the Gr-MoS_2 photodetector is a strong negative photoresponse at infrared wavelengths (which is much lower than the bandgap of single-layer MoS_2) and has been attributed to defects/traps in MoS_2 lying between the valence band and excitonic state [17]. Electron transport in graphene/MoS_2 heterostructures show negative compressibility when the MoS_2 conduction band is populated because of charge screening [19]. We draw motivation from the above studies and explore graphene as a sensor to study the effects of the underlying electronic band structure of tbl MoS_2. We observe some anomalies in the nature of electronic states in graphene and investigate the possible causes. Theoretical predictions as well as quantitative energy calculations suggest a possibility of these anomalies arising from effects of the moiré potential.

2. Experimental

Gr, MoS_2 and hBN were mechanically exfoliated using the scotch tape method onto a SiO_2/Si^{++} substrate. The number of layers of Gr and MoS_2 were identified by Raman Spectroscopy (details given in supplementary information). To fabricate a twisted structure, it is essential to know the atomic termination, i.e., if the flake edge is in a zigzag or in an armchair orientation. In MoS_2, it is known that if the angle between any two sharp edges is $\sim 60°$ or $\sim 120°$, that edge is zig-zag terminated [20]. This information helps us in the transfer process when fabricating the twisted structure. To obtain the desired twist angle in between two layers, we align the zig-zag edges accordingly. Figure 1a and b shows optical images of two monolayer MoS_2 flakes with sharp edges and edge angle of $\sim 60°$ with the zig-zag orientation marked. The optical images are then overlaid to create a design plan for a twist angle near 60° (see figure 1c). The image shows how the flakes need to be rotated and the zig-zag edges aligned to obtain a near 60° relative twist between the layers.

We used the dry transfer technique for fabricating the van der Waals heterostructures, which comprise of monolayer graphene, placed on top of a tbl MoS_2 with a bottom hBN layer (Gr-tbl MoS_2-hBN). The individual flakes are picked up successively on a sacrificial polymer layer spin-coated onto a PDMS drop placed on a glass slide. These are then transferred onto a pre-patterned SiO_2(285 nm)/Si(p-doped) substrate. The sacrificial layer is then dissolved in acetone. The process of aligning the layers is shown in the schematic of figure 1c. After capturing the first MoS_2 monolayer, we pick-up the second monolayer oriented exactly the same way as shown in the design plan by using a rotational stage. The twist angle between the two layers is thus determined during the transfer process. Post transfer, the angle can be observed optically as shown in figure 1d. This process, without the use of second harmonic generation to align the flakes and identify the twist angle is described elsewhere [21]. Determination of twist angle through optical images, introduces an error of 0.5°. Figure 1d shows the heterostructure after the transfer process with the zig-zag edges making an angle of 58.5° ± 0.5°. We have fabricated a near zero degrees tbl MoS_2, whose details are given in supplementary information. The twist angle determined optically is 3° ± 0.5°. The heterostructure with the outline of all the 2D layers is shown in figure 1e. We have also fabricated a control device with a natural bilayer (nbl) MoS_2 which is AB stacked (twist angle 60°). For device fabrication we use nanolithography technique. Electron beam lithography was used to create a channel solely on the tbl MoS_2 overlapped

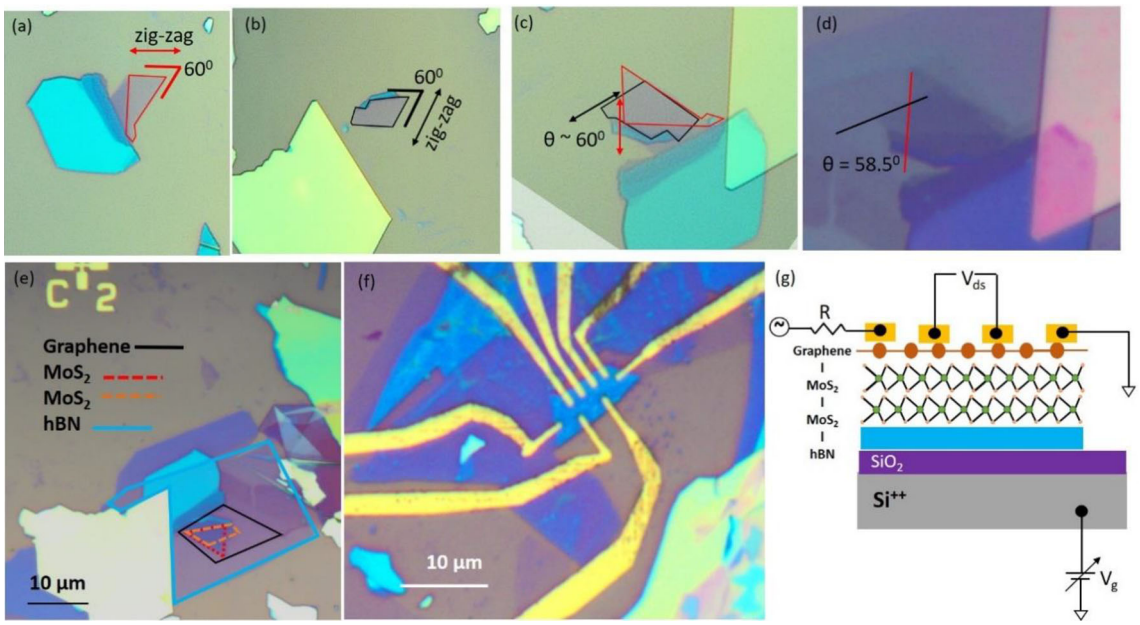

Figure 1. Fabrication of a twisted bilayer MoS_2 with a graphene sensing layer. (**a**) and (**b**) shows monolayer MoS_2 flakes with sharp edges making edge angle of $\sim 60°$, with the corresponding zig-zag edges marked. (**c**) Overlaid optical images of these two flakes showing the design plan for a transfer with twist angle near 60°. The flakes are rotated such that two zig-zag edges make a 60° angle. (**d**) The twisted bilayers after the transfer process; the two zig-zag edges make a 58.5° angle as determined from the optical image. (**e**) Optical image of the heterostructure showing Gr-MoS_2-MoS_2-hBN layers, which have been outlined for clarity. (**f**) Optical image of the device. (**g**) A schematic of the device showing the electrical circuit.

graphene region. Then Reactive-Ion-Etching using CHF_3 and O_2 plasma was used to etch out the remaining unwanted portion of the heterostructure. Electron beam lithography was performed again to fabricate Cr(5 nm)/Au(50 nm) electrical contacts onto graphene. An optical image of the device is shown in figure 1f and schematic of the measurement technique is given in figure 1g, described in the experimental section.

We have performed low temperature transport measurements by using a home-made dipstick inserted in cryofluid Helium wet bath. Electrical measurements were taken through automated program using LabView software via GPIB interface. We have used a constant current source by passing an ac sine voltage (0.1 V) from an SRS 830 Lock-in-Amplifier (LIA) through a resistor (1 MΩ). We measure the 4 probe or 2 probe voltages across the sample (electrical leads on the graphene) by LIA. The electrostatic back-gate doping is achieved through Keithley 2400 source meter, kept in voltage source mode.

3. Results

Figure 2a–c shows $(R - V_g)$ transfer characteristics of three trilayer hybrid devices, namely (a) graphene-natural bilayer (nbl), (b) graphene-MoS_2 bilayer twisted near 0° (tbl_n0°) and (c) graphene-MoS_2 bilayer twisted near 60° (tbl_n60°). All devices at 300 K show an asymmetric bell-shaped curve about the charge neutrality point (CNP), denoted by V_D. The asymmetry arises when V_g overcomes the threshold voltage (V_T) of MoS_2 (which is naturally n-doped). Beyond this value, even if V_g is increased, MoS_2 screens the charge carriers that leads to an almost fixed value of conductivity in graphene. Hence, a saturation is observed in the graphene conductivity. This is known as the screening effect and it pins the Fermi level (E_F) of graphene due to large number of available electronic states in MoS_2. At 300 K, the mobilities of the three devices lie between 1000 and 3000 $cm^2\ Vs^{-1}$. As we go to lower temperatures, the resistance of graphene at CNP increases. In tbl_n60°, the minimum conductivity at CNP (σ_{min}) at 10 K is $2.97 \times 10^{-4} \sim 7.5e^2/h$. In other devices, σ_{min} is slightly higher, by three to four times. The device parameters for all three samples are given in supplementary information. Figure 2d shows that σ_{min} increases by $\sim 30\%$ from 200 to 10 K. At lower temperatures ~ 10 K, the mobilities increase reaching upto a maximum of $\sim 8000\ cm^2\ Vs^{-1}$, which was observed in the tbl_n60°. The full-width half-maxima of the $(R - V_g)$ characteristics about the CNP gives an estimate of the carrier inhomogeneity (δn) in the system [22,23]. This inhomogeneity arises due to charged impurities and/or structural disorder, which can break the carrier system into puddles of electrons and holes. The upper limit for δn is $3.4 \times 10^{12}\ cm^{-2}$ at 10 K (in tbl_n60°). In monolayer graphene,

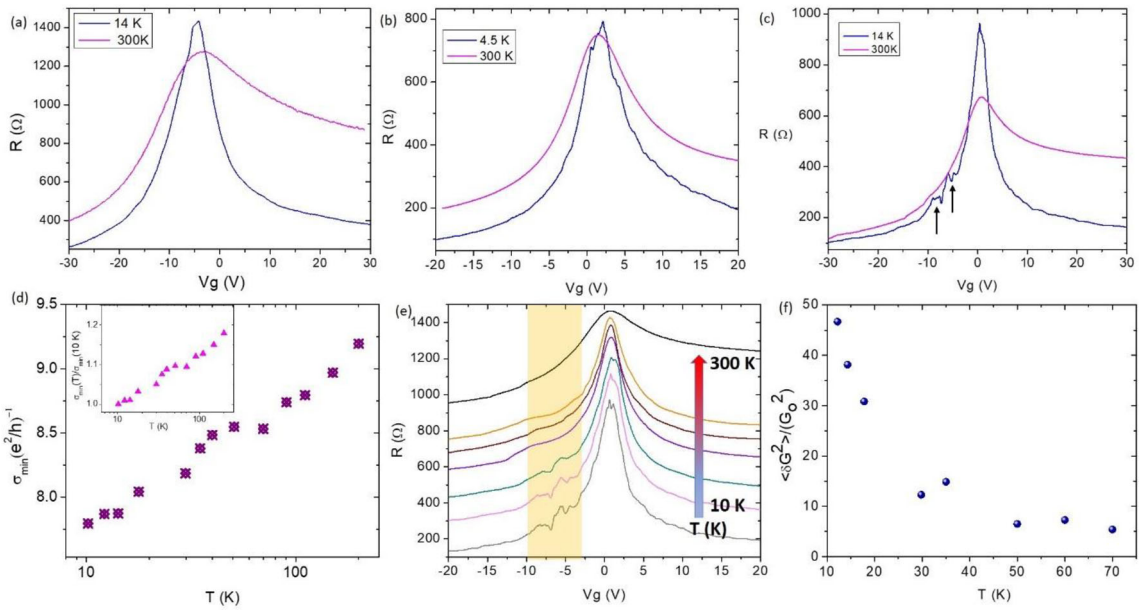

Figure 2. $R - V_g$ curves of three trinary hybrids at 300 K and at low temperature of graphene and (**a**) nbl MoS_2, (**b**) tbl_n0° and (**c**) tbl_n60°. The arrows indicate anomalous resistivity plateaus that were absent in devices based on nbl and that with twist angle close to 0°. (**d**) Variation of σ_{min} with temperature in tbl_n60°. Inset shows σ_{min} normalized to its value at $T = 10$ K as a function of temperature. (**e**) Temperature dependence of $R - V_g$ in tbl_n60° showing evolution of the plateau region. The curves have been shifted vertically for clarity. (**f**) Normalized conductance as a function of temperature for shaded region in part **e**.

σ_{min} has a significant temperature dependence only when, $k_B T \gg E_i$, where, $E_i \approx \hbar v_f \sqrt{\pi \delta n}$, is the rms chemical potential value of the charge puddle [22,23] and is equal to 2 meV. We can also calculate a lower limit for δn from σ_{min}, which is equal to $\sim 2.4 \times 10^{11}$ cm^{-2}. In an unencapsulated pristine monolayer graphene flake, the inhomogeneity varies between 2 and 9×10^{11} cm^{-2} [23]. The above analysis establishes that the devices have a low concentration of impurities in the graphene sheet and a satisfactorily high mobility suitable for further transport-related studies.

Figure 2c shows an anomalous feature in the $(R - V_g)$ curves as we go down to low temperatures ($\leq$ 15 K), in the tbl_n60° in the hole-doped region (marked by arrows). In contrast, the nbl (figure 2a) and the tbl_n0° (figure 2b) shows no such anomalies. In tbl_n60°, the resistance of graphene saturates for a small interval of V_g. These resistance plateaus lie between –9.5 V $< (V_g - V_D) <$ –8.0 V and – 6.4 V $< (V_g - V_D) <$ – 4.5 V. The evolution of the plateaus with temperature is shown in figure 2e. The two plateaus are distinct up to 35 K and merge into one plateau around 60 K onwards. In between the two plateaus, the graphene resistance drops sharply by $\sim$125 Ω. The corrugations in the data are repeatable for variable source currents ranging from 100 to 400 nA and over multiple cycles of data (see supplementary information).

In order to explore the features of $V_g \sim$ –5 to –9 V in the tbl_n60° (marked within the yellow shaded region in figure 2e) due to disorder-induced quantum interference effects, such as the Universal Conductance fluctuations (UCF), we study the corrugations in the data for estimating the magnitude of the fluctuations. A voltage range is chosen such that we include the plateau regions and capture the drop in graphene resistance. The $(R - V_g)$ data are fit to a polynomial function of order three and the variance of the residual of the fitted curve is calculated, which is $\langle \delta R^2 \rangle$. The magnitude of $\langle \delta G^2 \rangle$ is calculated from $\langle \delta G^2 \rangle = \langle \delta R^2 \rangle / \langle R \rangle^4$, where $\langle R \rangle$ is the mean value of the fitted curve [24]. Figure 2f shows the $\langle \delta G^2 \rangle / \langle Go^2 \rangle$ where Go is the quantum of conductance (e^2/h). The magnitude of fluctuations in this region is almost fifty times more than what we expect from UCF and their magnitude weakens with increasing temperature. This proves that the corrugations in the data have a different origin. These features could also arise from disorder-induced Coulomb blockade or charging effects. At low temperatures, the charge puddles that form as a result of disorder can act as a constriction to the conductance. The charging energy E_c associated with capacitance of the charge puddle can be determined by the width of the puddle D and is related by, $E_c = e^2/D$ [25]. If we assume that $E_c \approx E_i$, then the value of D we get is unreasonable ($\sim 10^{-10}$ nm). It is an unfeasible situation and we rule out the effects of Coulomb blockade. Thus, the source of these repeatable, periodic fluctuations at low temperatures do not arise from disorder-induced UCF, Coulomb blockade or charging effects and we speculate that it could originate from underlying effects of the moiré potential.

4. Discussions

In order to explore the anomalies that arise in the electronic states of graphene, we studied the electronic structure of tbl MoS_2 employing density functional theory. Tbl MoS_2 with twist angle close to 60° hosts several flatbands (bandwidth <1 meV) at the conduction band edge [3,14]. This occurs due to a deep confining potential well at the Bernal stacking region, where the Mo atom is on top of Mo and the S atom is on top of the hollow of the hexagon. The flatbands near the conduction band edge localize on this stacking and as the twist angle approaches 60°, the flatbands appear deeper in the bandgap of MoS_2. Figure 3e gives the electronic band structure of tbl MoS_2 at 58.5° with distinguishable flatbands labelled from C1 to C6. Furthermore, these flatbands are two or four or six-fold degenerate, which result in large density of states (DOS) at a particular energy level. We show the DOS of 58.5° tbl MoS_2 in figure 3c. It shows several distinguishable peaks at the conduction band edge. For comparison, we have also shown the DOS due to a nbl in the shaded region. Clearly, the flatbands start appearing at lower energy values than the conduction band edge of the nbl MoS_2. Note that the vacuum level is set to zero for both the DOS plots. On the other hand, the flat bands at conduction band edge in tbl MoS_2 with twist angle close to 0°, have finite dispersion but the energy separation between them is small. As a result, the DOS at the conduction band edge does not show any distinguishable peak (see figure 3d).

We propose that the plateaus in the graphene resistance with changing electrostatic doping could possibly arise from Fermi level pinning due to the presence of large DOS in tbl_n60°. As discussed above, tbl MoS_2 with twist angles near 60° hosts ultra-flatbands below the conduction band edge. We speculate that the presence of these flatbands below the conduction edge of MoS_2 provides the necessary large number of electronic energy states that screens the backgate voltage. This leads to Fermi level pinning and the conductance in Gr remains unchanged. Once V_g goes beyond the flatband energy level, the conductance of Gr shows a sharp drop since the fermi level (E_F) in Gr shifts suddenly. A schematic is shown in figure 3a to better visualize the phenomena. To elucidate this proposition, we proceed to calculate the energy levels in the trinary hybrid system.

The total carrier density (n_T) of the grapehe-MoS_2 heterostructure is given by [19],

$$n_T = n_g + n_M = \frac{C}{e}(V_g - V_D), \tag{1}$$

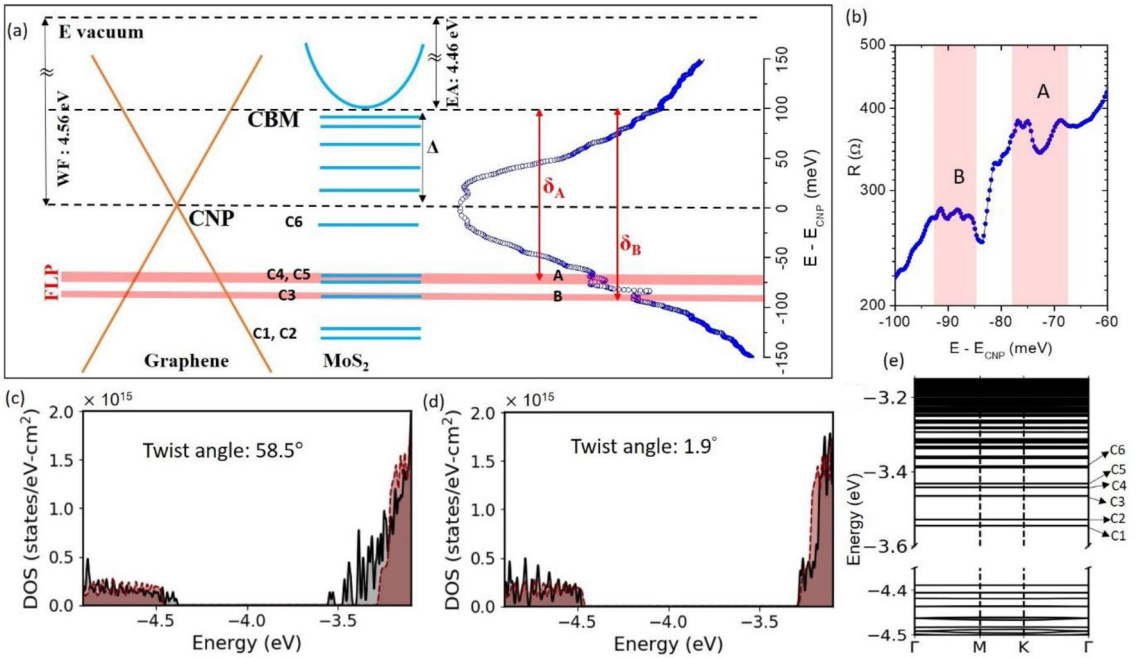

Figure 3. (**a**) Schematic of the band alignment in graphene-tbl MoS_2 heterostructure with twist angle of 58.5°. The flatbands are indicated as blue lines below the CBM of MoS_2. The Fermi level pinning positions have been marked, which occurs when chemical potential of graphene aligns with a flatband. The $(R - E)$ data are given alongside for better visualization of the proposed model. The flatbands are indicated from C1 to C6. The energetical positions are not to scale. (**b**) The magnified view of the $(R - E)$ plot in the region of anomalies with regions *A* and *B* marked and shaded. (**c**, **d**) Theoretically calculated density of states of 58.5° and 1.9° tbl MoS_2, respectively. The shaded region corresponds to the DOS of nbl MoS_2. (**e**) Magnified view of the calculated band structure of tbl MoS_2 at 58.5° with flatbands C1 to C6 marked alongside.

where, n_g and n_M are the carrier densities of graphene and MoS_2, respectively, C is the capacitance per unit area of the gate oxide (285 nm of SiO_2 and 12 nm of hBN, which gives C = 119 μF m^{-2}) and e is the electron charge. It is known that the exchange energy and correlation energy on the chemical potential of MoS_2 leads to negative quantum capacitance, resulting in a capacitive effect which alters the total gate capacitance [19]. To accurately calculate the carrier density of graphene, we use an effective gate capacitance (C_{eff}), defined as,

$$n_g = \frac{C}{e}(V_g - V_D) - n_M = \frac{C_{eff}}{e}(V_g - V_D) \quad (2)$$

For monolayer MoS_2, it has been seen that the many-body effects on the chemical potential of MoS_2 can alter the gate capacitance by ∼10 μF m^{-2} (supplementary information). Using the effective gate capacitance and the relation, $E = \pm\hbar v_F\sqrt{\pi n_g}/e$ where, the Fermi velocity v_F = 10^6 cm s^{-1} in graphene, we convert the back-gate voltage to energy. The $R - (E - E_{CNP})$ plot in the region of interest of the two plateaus marked A and B is given in figure 3b, where E_{CNP} is the energy at CNP.

The band offset (Δ) between graphene and MoS_2 depends on the number of layers, doping, disorder, dielectric environment, etc. [19]. The characteristic $(R - V_g)$ curve of graphene shows electron–hole asymmetry from conductivity saturation on the electron side, which signals the onset of population in the MoS_2 conduction band $(V_g \geq V_T)$. At this point, the chemical potential of electrons in graphene is in alignment with the bottom of the conduction band of MoS_2. From the electron–hole asymmetry (see supplementary information) we determine the energy offset between the Dirac point of graphene and the conduction band minima (CBM) of MoS_2. It is 100 ± 3 meV and is shown in the schematic of figure 3a. The electron affinity (χ_M) of MoS_2 can be calculated from here, $\Delta = \phi_G - \chi_M$, [19] where, ϕ_G ≈ 4.56 eV is the work function of graphene [26]. Using this equation, χ_M of tbl MoS_2 is ≈ 4.46 eV. Monolayer MoS_2 has χ_M equal to 4.7 eV, while nbl MoS_2 has χ_M equal to 4.4 eV [27]. The value of χ_M which we determine from the band offset, using the asymmetry in electron–hole branches, is thus in good agreement with established data. The energy widths of the plateaus in regions *A* and *B* are 12.2 ± 0.6 and 10.4 ± 1.1 meV, respectively (see figure 3b). Additionally, we determine how far in energy the CBM lies from these points, which we denote by δ. From point *A* we get, δ_A = 172 ± 5 meV and from point *B* we get δ_B = 189 ± 6 meV. The separation between the mid-points of these two plateaus is ∼17 ± 1.7 meV. From theoretical calculations in a 58.5° tbl MoS_2, we see that multiple flatbands lie upto ∼300 meV below the conduction band continuum. The first few flatbands are very close to the CBM, beyond which, the energy separation between two consecutive flatbands increases. It is also essential to identify the conduction band edge from the DOS/band structure calculations in a tbl MoS_2. The qualitative identification of the CBM is given supplementary information. The energetical positions of the isolated flatbands C1, C2, C3, C4, C5 and C6 below CBM are 305, 290, 225, 200, 191 and 147 meV (see figure 3e and supplementary figure). The separation between the flatbands are as follows: C1–C2 = 15 meV, C2–C3 = 65 meV, C3–C4 = 25 meV, C4–C5 = 9 meV and C5–C6 = 44 meV.

The correlation between the calculated flatband position and the experimental results is encouraging. We may point out that energetical positions of C3, C4 and C5 are similar to the value of δ_A and δ_B. The separation between *A* and *B* is ≈ 17 meV, which is approximately equal to C3–C4, considering thermal broadening effects. It should be noted that we were able to access only upto 250 meV below the CBM, hence any features due to flatbands beyond this region (C1 and C2) have not been captured experimentally. Our experimental results also show that no anomalies appear in the 3° bilayer MoS_2, which is consistent with the theoretical calculations that show no well-separated bands are present below the CBM in the tbl MoS_2 near 0°. Other flatbands are not observed in the transport through graphene since they lie very close to CNP. Due to disorder-induced charge-puddle formation in graphene around the Dirac point, we were not able to observe these anomalies. Other factors include localization at the band tail of MoS_2 (due to defect states in MoS_2) [28] and formation of a mobility edge [29] that prevents gate-voltage screening by the flatbands of MoS_2 that lie near the MoS_2 conduction band edge. Thus, even though flatbands are present, we are not able to resolve them experimentally.

The schematic in figure 3a provides an account of band alignments in a graphene-twisted-MoS_2 heterostructure. It represents the position of flatbands in MoS_2 with respect to graphene. The flatbands, which lie energetically below the Dirac point of graphene, and in the bandgap of MoS_2 enables us to experimentally observe its effect on the electronic states of graphene. We suggest a possible outcome of the manifestation of the flatbands in a graphene-tbl MoS_2 hybrid as a pinning of the Fermi level when the chemical potential of graphene aligns with a flatband.

5. Conclusion

In summary, we use graphene as a sensing layer to study emergent phenomenon in a tbl TMDC. The electronic states in the graphene-MoS_2 hybrid, with the MoS_2 layers forming a MSL with a twist angle at 58.5°, show anomalies at low temperatures. Interestingly, these features appear only in the near 60° MSL and not on the 3° twisted device or on the natural bilayer devices. We have ruled out the effects of UCF and Coulomb blockade based on electrical characterization of the trinary hybrids and suggest a possibility that the anomalies arise from interactions with the underlying moiré potential. Theoretical calculations show multiple

isolated flatbands near the conduction band edge of bilayer MoS_2 for twist angles near 60°. We speculate that as the chemical potential of graphene aligns with the flatbands, their large density of states pins the fermi level of graphene, which leads to the observed plateaus in resistance. We calculate the energy values of the position of these anomalies with respect to the conduction band edge of MoS_2, and they are in quantitative agreement with the predicted energy levels for flatbands in tbl MoS_2 with a twist angle of 58.5°. Our work illustrates a unique approach to observe flatband phenomenon in twisted TMDCs.

Acknowledgement

We acknowledge financial support from the U.S. Army International Technology Centre Pacific (ITC-PAC) and Ministry of Electronics and Information Technology, Government of India, as well as the Supercomputer Education and Research Centre (SERC) at IISc, for providing computational resources. SS acknowledges Aditya Jayaraman for fruitful discussions during the development of the work.

References

[1] Yu H, Liu G B, Tang J, Xu X and Yao W 2017 *Sci. Adv.* **3** e1701696
[2] Bistritzer R and MacDonald A H 2011 *Proc. Natl. Acad. Sci.* **108** 12233
[3] Naik M H and Jain M 2018 *Phys. Rev. Lett.* **121** 266401
[4] Kundu S, Naik M H, Krishnamurthy H R and Jain M 2021 arXiv:2103.07447
[5] Chen G, Jiang L, Wu S, Lyu B, Li H, Chittari B L *et al* 2018 *Nat. Phys.* **15** 237
[6] Jin C, Regan E C, Yan A, Utama M I B, Wang D, Zhao S *et al* 2019 *Nature* **567** 76
[7] Tran K, Moody G, Wu F, Lu X, Choi J, Kim K *et al* 2019 *Nature* **567** 71
[8] Cao Y, Luo J Y, Fatemi V, Fang S, Sanchez-Yamagishi J D, Watanabe K *et al* 2016 *Phys. Rev. Lett.* **117** 116804
[9] Cao Y, Fatemi V, Fang S, Watanabe K, Taniguchi T, Kaxiras E *et al* 2018 *Nature* **556** 43
[10] Pan H, Wu F and Sarma S D 2020 *Phys. Rev. Res.* **2** 033087
[11] Zhang Z, Wang Y, Watanabe K, Taniguchi T, Ueno K, Tutuc E and LeRoy B J 2019 arXiv:1910.13068
[12] Wang L, Shih E M, Ghiotto A, Xian L, Rhodes D A *et al* 2020 *Nat. mater.* **19** 861
[13] Xu Y, Liu S, Rhodes D A, Watanabe K, Taniguchi T, Hone J *et al* 2020 *Nature* **587** 214
[14] Naik M H, Kundu S, Maity I and Jain M 2020 *Phys. Rev. B* **102** 075413
[15] Roy K, Padmanabhan M, Goswami S, Sai T P, Ramalingam G, Raghavan S *et al* 2013 *Nat. Nanotech.* **8** 826
[16] Mitra S, Kakkar S, Ahmed T and Ghosh A 2020 *Phys. Rev. Appl.* **14** 064029
[17] Ahmed T, Roy K, Kakkar S, Pradhan A and Ghosh A 2020 *2D Mater.* **7** 025043
[18] Kashid R, Mishra J K, Pradhan A, Ahmed T, Kakkar S, Mundada P *et al* 2020 *APL Mater.* **8** 091114
[19] Larentis S, Tolsma J R, Fallahazad B, Dillen D C, Kim K, MacDonald A H *et al* 2014 *Nano Lett.* **14** 2039
[20] Guo Y, Liu C, Yin Q, Wei C, Lin S, Hoffman T B *et al* 2016 *ACS Nano* **10** 8980
[21] Debnath R, Sett S, Biswas R, Raghunathan V and Ghosh A 2021 *Nanotech.* **32** 455705
[22] Dean C R, Young A F, Meric I, Lee C, Wang L, Sorgenfrei S *et al* 2010 *Nat. Nanotech.* **5** 722
[23] Bolotin K I, Sikes K J, Hone J, Stormer H L and Kim P 2008 *Phys. Rev. Lett.* **101** 096802
[24] Pal A N, Kochat V and Ghosh A 2012 *Phys. Rev. Lett.* **109** 196601
[25] Sols F, Guinea F and Neto A C 2007 *Phys. Rev. Lett.* **99** 166803
[26] Yan R, Zhang Q, Li W, Calizo I, Shen T, Richter C A *et al* 2012 *Appl. Phys. Lett.* **101** 022105
[27] Howell S L, Jariwala D, Wu C C, Chen K S, Sangwan V K, Kang J *et al* 2015 *Nano Lett.* **15** 2278
[28] Kunstmann J, Wendumu T B and Seifert G 2017 *Phys. Status Solidi (b)* **254** 1600645
[29] Mongillo M, Chiappe D, Arutchelvan G, Asselberghs I, Perucchini M, Manfrini M *et al* 2016 *Appl. Phys. Lett.* **109** 233102